JOURNAL OF PROPULSION AND POWER
Vol. 14, No. 5, September–October 1998

Mixing and Spray Formation in Coaxial Jets

Emmanuel Villermaux*
Centre National de la Recherche Scientifique, BP 53X, 38041 Grenoble Cedex, France

The flow regimes and fine-scale structure of the mixture resulting from the destabilization of a dense, slow jet by a fast light annular jet are discussed. From the primary shear instability between the streams, it is shown that the momentum ratio $M = \rho_2 u_2^2/\rho_1 u_1^2$ of the annular to the inner stream is the key parameter on which the inner potential core length and the condition of a recirculation transition depend. The instability analysis shows that the initial wavelength of the disturbances λ is proportional to the vorticity thickness δ of the fast stream at the nozzle exit $\lambda \sim \delta(\rho_1/\rho_2)^{1/2}$; this further provides, by an original scenario, an estimate of the droplets' size formed by the capillary instability of the sheet's rim formed from the initial interface disturbances. Liquid viscosity is not expected to play any significant role in practical conditions in liquid rocket propellant engines. These findings are put in relation with a selected review of known or yet unexplained results on the subject.

I. Introduction

THERE is a frequent need to realize a uniform mixture from two initially segregated streams in many practical instances. A significant example is the case of liquid rocket propellant engines because the length of the combustion chamber is limited by the ability of the injecting devices to fragment and mix the reactants down to a sufficient level of homogeneity for evaporation and combustion to completion at the desired distance from the injector outlet.

For technological reasons one of the reactants is usually available in the liquid state and the other in the gas phase; for historical reasons the coaxial geometry is commonly used to merge the two streams.[1] The relative flow rates of the reactants must be adjusted so that the global stoichiometry is at least respected, or such that the gas phase is in excess for all of the liquid to vaporize and burn, this implies that the gas stream is usually much more rapid than the liquid stream at the injector outlet. This is the situation encountered in H_2/O_2 engines, where a slow, dense liquid oxygen (LOX) stream in the central jet of the coaxial injector is surrounded by a fast, light, gaseous hydrogen annular stream.

At the root of the interpenetration process between the two phases is a strong shear destabilizing the central liquid jet, which further fragments into a more or less uniform spray. This process, which is contrasted with the case of a simple jet issuing in a quiescent environment,[2] is known as airblast atomization.[3]

The subject matter has been extensively reviewed in the precise context of atomization and combustion in rocket engines.[4,5] In this paper we provide new facts and a renewed, consistent picture of both the global entrainment rate of the slow phase by the fast one, but also of the primary droplet formation mechanism and resulting fine structure of the mixture. This originates in a detailed investigation of the basic instability involved and of the relevant ingredients that determine its growth rate and wavelength; its exposition is discussed in Sec. II. In Sec. III the different flow regimes of the coaxial configuration are discussed; the inner potential core-length dependency (or liquid intact length) to the external parameters and the conditions of the recirculation transition, and the formation of a wake-type bubble downstream of the inner jet exit. The fine structure of the resulting mixture and the mechanism of droplet formation are discussed in Sec. IV. The experimental evidence presented, both in homogeneous flows and in liquid-gas configurations, leads to the proposal of a limited number of scenarios for primary droplet formation relevant to practical conditions.

Received Sept. 2, 1997; revision received Feb. 12, 1998; accepted for publication March 19, 1998.

*Laboratoire des Ecoulements Géophysiques et Industriels. E-mail: villerma@hmg.inpg.fr.

II. Shear Instability Mechanism: Entrainment Rate and Wavelength

A. Entrainment Rate

Consider Fig. 1.[6] The photographs represent the destabilization of a central water jet by a cocurrent annular water stream. The velocity ratio between the annular jet (subscript 2) and the inner one (subscript 1) is $r_u = u_2/u_1 = 3$ to 4, which corresponds to a momentum flux ratio $M = \rho_2 u_2^2/\rho_1 u_1^2$, a key quantity for the near-field geometry of coaxial configurations of about 10. The fact that the flow does not involve a difference of phase, thus ruling out the possible role of surface tension, is of no importance as far as the inner potential core length and the wavelength determination of the primary shear instability are concerned.

Before the interfacial instability mechanism is discussed, a simple qualitative argument is presented that provides the global entrainment rate from the slow toward the rapid phase. Let λ be the wavelength of the interface corrugation, with amplitude ξ (Fig. 1). Because of incompressibility, the velocity field is perturbed on a length scale of the order of λ in a direction perpendicular to the interface. If $u_2(x)$ denotes the fast stream velocity in the vicinity of the interface, mass conservation on the fast stream side reads

$$u_2(x)\lambda \approx u_2(x + \lambda/2)[\lambda - \xi] \tag{1}$$

thus expressing the acceleration of the fluid on the crests of the interface corrugations and deceleration in the hollows. The conservation of energy along a streamline provides, according to Bernoulli's equation in the high-Froude-number limit, the resulting pressure difference Δp

$$\Delta p = |p(x) - p(x + \lambda/2)| \approx \tfrac{1}{2}\rho_2 u_2^2(\xi/\lambda) \tag{2}$$

expressing the self-amplified character of shear instabilities.

The growth rate $r = \dot{\xi}/\xi$ of the instability is readily estimated by a force/unit length balance in the direction perpendicular to the interface

$$\underbrace{\rho_1\lambda^2}_{\text{mass/length}} \times \underbrace{r^2\xi}_{\text{acceleration}} \sim \underbrace{\Delta p\lambda}_{\text{driving force/length}} \tag{3}$$

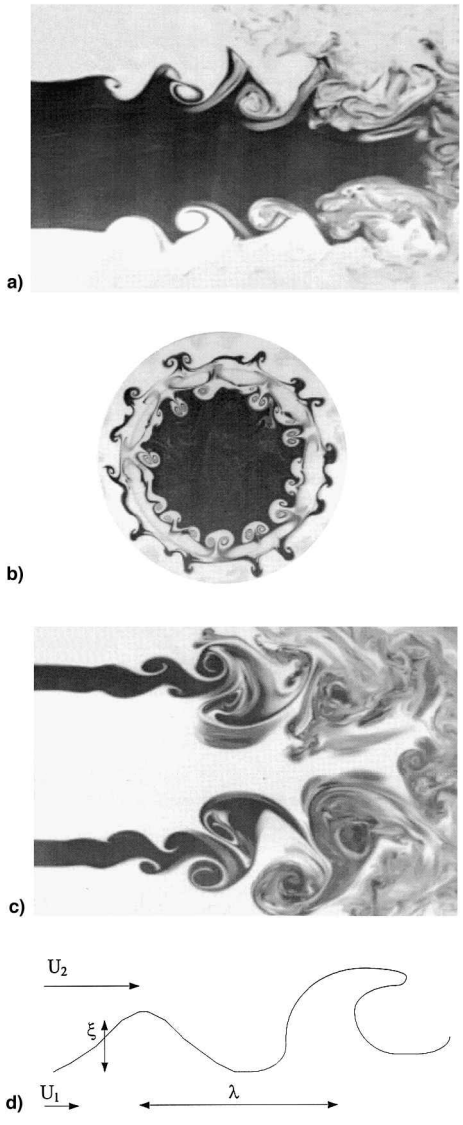

Fig. 1 Instantaneous planar cuts of the flow structure of water–water coaxial jets. One of the streams is seeded with a fluorescent dye (adapted from Rehab et al.[6]): a) central jet is seeded and the laser light sheet passes through the axis of the jets, $r_{\mu} = 3$; b) cut in the transverse direction one diameter downstream of the injectors outlet, $r_{\mu} = 4$; c) outer jet seeded, $r_{\mu} = 4$; and d) sketch of the interface destabilization process.

The time needed for an instability structure of linear scale λ to increase to a size where it is either diluted in the rapid stream by stretching enhanced diffusion, or removed from the interface when a break-up mechanism is present (see Sec. IV) is of the order of $1/r$. This time scale is usually the limiting time step of the entrainment process. The entrainment velocity $u_e \approx r\lambda$ thus writes, when $u_2 >> u_1$ and according to Eqs. (2) and (3)

$$u_e \approx r\lambda \sim u_2(\rho_2/\rho_1)^{1/2} \tag{4}$$

This result is important for two reasons. First, it incorporates a nontrivial dependency on the density ratio ρ_2/ρ_1 between the phases. The 1/2 power comes from the square dependency of the pressure difference Δp on the shear velocity u_2, i.e., $\Delta p \sim \rho_2 u_2^2$, and is a common feature of all inertial instabilities whose destabilizing ingredient is a velocity difference. Second, and more important, the entrainment velocity derived in Eq. (4) has a scale invariant form and holds whatever λ may be. In other words, whatever the physical process that fixes the absolute value of the instability length scale λ, the entrainment velocity will always have the form indicated in Eq. (4) as soon as the destabilizing process is caused by shear. The discussion concerning the stabilizing ingredients of the instability leading to its wavelength is completely disconnected from the estimation of the entrainment rate u_e.

B. Instability Wavelength

Once the destabilizing role of the shear is recognized, it is easy to go one step further and formulate a complete instability problem to consider a pure velocity discontinuity at the interface and to seek a restoring mechanism for the selection of the mode linked with the physical properties of the fluids, namely surface tension of the liquid.

This point of view was first proposed by Taylor,[7] who was, in fact, mainly looking for the entrainment velocity u_e derived in Eq. (4). Many reformulations have appeared since then in the context of airblast atomization, high-speed gas-assisted spray formation, and in this context this representation is usually admitted to be at the source of droplet formation.[4]

This approach to the problem could be called the Kelvin–Helmholtz paradigm, after von Helmholtz,[8] who first pointed out the destabilizing role of the velocity discontinuity, and then Kelvin,[9] who performed thorough calculations deriving the stability curve, including capillary and gravity effects. Expanding the liquid-gas interfacial disturbances in Fourier modes as $\xi \sim \exp(ikx - i\omega t)$, the dispersion relation, neglecting gravity (high-Froude-number limit), is

$$(\rho_1 + \rho_2)\omega/k = \rho_1 u_1 + \rho_2 u_2 \pm \sqrt{(\rho_1 + \rho_2)\sigma k - \rho_1\rho_2(u_2 - u_1)^2} \tag{5}$$

where σ stands for the surface tension of the liquid.[10,11] The relative motion is always destabilizing and the surface tension stabilizes the interface at small scale for

$$k > k_c = \frac{\rho_1\rho_2}{\rho_1 + \rho_2}\frac{(u_2 - u_1)^2}{\sigma}$$

In the practical limit where $\rho_1 >> \rho_2$ (liquid-gas) and $u_2 >> u_1$ (strong shear), the maximal growth rate r and its associated most amplified wavelength are

$$r = (2/3\sqrt{3})(\rho_2/\rho_1)^{1/2}(\rho_2 u_2^3/\sigma) \tag{6a}$$

$$\lambda = 3\pi(\sigma/\rho_2 u_2^2) \tag{6b}$$

Note that, as expected from the considerations of Sec. II.A, the product $r\lambda$ that identifies the entrainment velocity u_e is found to be proportional to $u_2(\rho_2/\rho_1)^{1/2}$. The physical ingredients underlying this result that are derived exactly in this form by Caré and Ledoux,[12] and because of the determinant role played by surface tension as the stabilizing ingredient, predict that the wavelength λ depends linearly on the value of the surface tension σ, and is a strong decreasing function of the gas-phase velocity, i.e., ${u_2}^{-2}$. A similar result accounting for the finite size of the liquid-injection thickness sandwiched between two high-speed airstreams was derived by Squire.[13] When the initial sheet thickness is comparable to λ given by Eq. (6b), the instability selects a sinuous mode that confers a wavy pattern to the sheet.

This result is, however, in most laboratory experiments and for most actual injection conditions inappropriate. The reason for this is that the only way to produce a shear between two parallel streams is to accelerate them in distinct channels separated by a rigid boundary (a splitter plate for mixing layers, the central tube in coaxial jets etc.), and to make them merge downstream of the splitter lip. The method implies the formation of boundary layers at the wall of the conveying channels resulting in the continuity of the velocity profile across the interface separating the two streams at their merging location (Fig. 2).

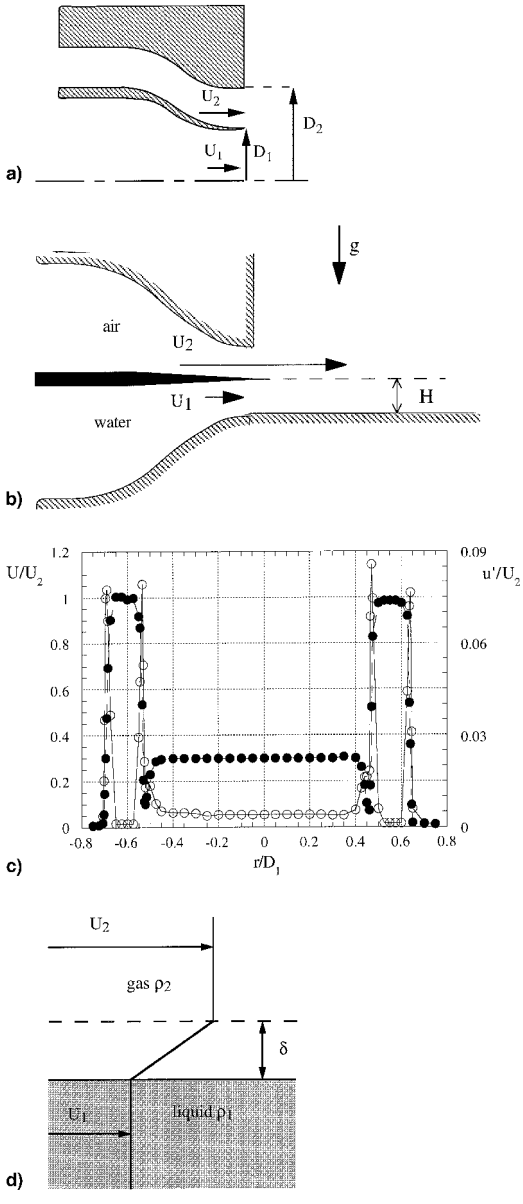

Fig. 2 Experimental configurations and exit conditions: a) coaxial jet nozzle, D_1, D_2, u_1, and u_2 are the diameters and centerline exit velocities of the inner and outer jets, respectively, $D_1 = 4$ cm, $D_2 = 5.5$ cm; b) plane air/water mixing layer; c) radial profiles of mean velocity (●) and rms values (○) of the velocity fluctuations in the exit plane of the coaxial jets, $r_u = 3$ (note the vorticity thickness on the mean velocity profile); and d) sketch of the initial density and velocity profiles.

In addition to the length scale formed by the ratio of the surface tension to the inertia of the gas $\sigma/\rho_2 u_2^2$, a new length scale appears, namely the thickness of the boundary layers at the splitter lip δ (Fig. 2d). Extending the Kelvin and Helmholtz approach, the first analysis of this question is from Rayleigh,[14] who investigated the stability properties of a piecewise linear velocity profile in a constant density, homogeneous flow. Letting δ be the thickness of the shear layer, and introducing the dimensionless quantities $\kappa = k\delta$ and $\Omega = \omega/k(u_2 - u_1)$, the dispersion relation was found by Rayleigh in the form

$$e^{-2\kappa} = [1 - \kappa(2\Omega + 1)][1 + \kappa(2\Omega - 1)] \tag{7}$$

The layer is unstable for all wave numbers such that $k\delta < 1.28$, and the maximal growth rate, corresponding to $k_m\delta \approx 0.8$ is such that $r \approx 0.2(u_2 - u_1)/\delta$. The numerical factors are only slightly sensitive to the detailed shape of the velocity profile (see, e.g., Esch[15] and Monkewitz and Huerre[16]), so that the piecewise linear profile is actually a generic caricature. The important feature of the dispersion relation is that the layer is transparent to the shear for wavelengths smaller than about the initial width δ [exactly $(2\pi/1.28)\delta$].

The instability analysis can be performed in the presence of density differences between the phases (see, e.g., Pouliquen et al.[17] and references therein), possibly incorporating surface tension[18] and has an analytical form in the high-Froude and Weber-number limit[19]

$$e^{-2\kappa} = [1 - \kappa(2\Omega + 1)] \frac{1 + \kappa \dfrac{(\rho_1/\rho_2) + 1}{2}(2\Omega - 1)}{1 + \kappa \dfrac{(\rho_1/\rho_2) - 1}{2}(2\Omega - 1)} \tag{8}$$

which reduces to Eq. (7) for $\rho_1/\rho_2 = 1$. The dispersion relation [Eq. (8)] is obtained when the shear is entirely located in the rapid, light phase (Fig. 3). One can indeed show that the velocity profile that develops in the slow phase by vorticity diffusion and continuity of the stress at the interface does not affect the instability based on the fast stream characteristics only. The velocity profile induced in the slow phase reaches an appreciable thickness such that its own instability is no more damped by viscosity in a time scale that is larger than the instability development time scale of the initial profile of Fig. 2d, and this occurs even for very large-density ratios ρ_1/ρ_2.[20]

For increasing density ratios, ρ_1/ρ_2, the instability is progressively damped. It is, however, never suppressed, except for the infinite density ratio, a case that amounts to the linear boundary-layer profile over a rigid plate known to be linearly stable in the inviscid limit.[21] The cutoff wave number k_c as well as the most amplified mode k_m and its associated growth rate decrease accordingly, leading to a preferred wavelength λ that becomes larger and larger as ρ_1/ρ_2 increases.

According to the general principle outlined in Sec. II.A, the product of the maximal growth rate r to the selected wavelength λ always remains essentially proportional to $u_2(\rho_2/\rho_1)^{1/2}$.

The individual evolutions of r and λ with ρ_1/ρ_2 can, in turn, be extracted from Eq. (8) by a special procedure. Noticing that a change in the density ratio roughly results in a multiplicative factor on both axes of the dispersion curve as shown on Fig. 3b, one may map the different curves on top of each other by a linear transformation on Ω and κ involving two multiplicative functions $F(\rho_1/\rho_2)$ and $G(\rho_1/\rho_2)$ of the density ratio as

$$\kappa = F(\rho_1/\rho_2)\kappa' \tag{9a}$$

$$\Omega = G(\rho_1/\rho_2)\Omega' \tag{9b}$$

the transformed dimensionless wave number and frequency κ' and Ω' being now linked by the dispersion relation of the homogeneous case [Eq. (7)]. The expansions of Eqs. (7) and (8) coincide up to the second order in κ, provided the functions F and G have the form

$$F\frac{\rho_1}{\rho_2} = \frac{5}{6} - \frac{1}{6(\rho_1/\rho_2)} + \frac{\sqrt{5 + 13(\rho_1/\rho_2) - 37(\rho_1/\rho_2)^2 + 27(\rho_1/\rho_2)^3}}{6\sqrt{2}(\rho_1/\rho_2)} \tag{10a}$$

$$G\frac{\rho_1}{\rho_2} = \frac{1 + (\rho_1/\rho_2)}{2\sqrt{\rho_1/\rho_2}} \tag{10b}$$

Equations (10a) and (10b) thus allow a continuous representation of the growth rate

$$r \approx \frac{0.2}{F(\rho_1/\rho_2)G(\rho_1/\rho_2)} \frac{u_2 - u_1}{\delta} \xrightarrow{\rho_1/\rho_2 > 10} \frac{\rho_2}{\rho_1}\frac{u_2}{\delta} \tag{11a}$$

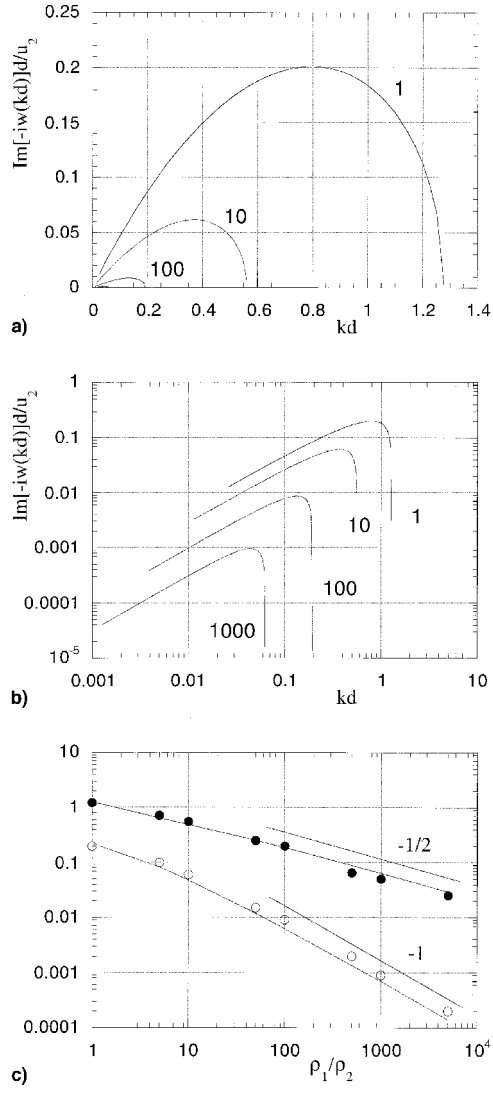

Fig. 3 a) Dispersion curves [Eq. (8)] of the inviscid linear instability of the piecewise linear velocity profile of Fig. 2d for increasing density ratio ρ_1/ρ_2 (from Villermaux[19]); b) same as in part a) but with log–log scales; and c) maximal amplification rates $r\delta/u_2$ (○) and cutoff wave numbers $k_c\delta$ (●) vs density ratio ρ_1/ρ_2. The continuous lines are the fits from the functions F and G of Eq. (10).

and selected wavelength

$$\lambda = \frac{2\pi}{0.8} F \frac{\rho_1}{\rho_2} \delta \xrightarrow{\rho_1/\rho_2 > 10} \frac{2\pi}{1.5} \left(\frac{\rho_1}{\rho_2}\right)^{1/2} \delta \qquad (11b)$$

in an approximate, but accurate form. As soon as $\rho_1/\rho_2 > 10$, r and λ nearly follow a pure power law on the density ratio (Fig. 3c).

The reason why particular attention is paid to the stability limits in the presence of a finite size shear-layer thickness δ is now clear: The shear does not affect the layer for wavelengths smaller than λ given by Eq. (11b); the Kelvin–Helmholtz destabilizing mechanism is thus suppressed in this range of scales. The mode selected by the instability will thus, even in the presence of surface tension, be the one predicted by Eq. (11b) solely as soon as the wavelength [Eq. (11b)] is larger than the wavelength of the pure Kelvin–Helmholtz mechanism [Eq. (6b)]. This condition reads

$$\delta(\rho_1/\rho_2)^{1/2} > \sigma/\rho_2 u_2^2 \qquad (12a)$$

that is

$$We(\rho_1/\rho_2)^{1/2} > 1 \qquad (12b)$$

where $We = \rho_2 u_2^2 \delta/\sigma$ is the Weber number based on the initial fast-stream, boundary-layer thickness. Equation (12b) is fulfilled in the majority of laboratory conditions at atmospheric pressure, and is reached by far in high-pressure combustion chambers. The viscosity of the liquid does not play any damping role on the development of the instability as long as $\lambda^2/\nu_1 >> \lambda/u_e = r^{-1}$, that is, $(\nu_2/\nu_1)(u_2\delta/\nu_2) >> 1$, a condition that is fulfilled in most circumstances.

The fact that the scale of the primary instability is determined by the exit conditions of the velocity profile is obvious from one-phase experiments as shown in Fig. 1, and has been established by Rehab et al.[22]

This result was further demonstrated in the two-phase, liquid-gas plane shear-layer configuration of Fig. 2 by Raynal et al.[23] (also see Lasheras et al.[24]). These authors were able to show that the interface destabilization frequency measured downstream from the splitter plate in the region of the primary instability development indeed scales as the group velocity $u_c = \partial/\partial k(Re[\omega(k)])$, divided by the vorticity thickness δ of the gas-phase velocity profile at the splitter lip [the instability wavelength λ is proportional to δ, see Eq. (11b)]

$$f = (u_c/\lambda) \sim (u_c/\delta)(\rho_2/\rho_1)^{1/2} \qquad (13)$$

Comparison of the measured frequency with the present linear stability analysis was found to be in good numerical agreement, consistent with the generic character of the piecewise linear profile for shear instabilities (Fig. 4). Raynal et al.[23] were also able to directly measure the group velocity u_c in their experiment. In the high-momentum-ratio M limit, u_c is essentially proportional to the high-speed gas velocity with a prefactor involving the square root of the density ratio as for entrainment velocity. The group velocity can be precisely computed from Eq. (8) and is consistent with a useful, a priori estimate grounded on momentum transfer arguments[25]

$$u_c \approx \frac{\sqrt{\rho_1}u_1 + \sqrt{\rho_2}u_2}{\sqrt{\rho_1} + \sqrt{\rho_2}} \xrightarrow{M>>1} u_2 \left(\frac{\rho_2}{\rho_1}\right)^{1/2} \qquad (14)$$

Note that the dependencies of u_c on ρ_1 and ρ_2 are here substantially different from the ones derived from the pure Kelvin-Helmholtz mechanism [Eq. (5)] for which $u_c = (\rho_1 u_1 + \rho_2 u_2)/(\rho_1 + \rho_2)$.

This is, together with the fact that the interface destabilization frequency was observed to be unaffected by varying surface tension and viscosity of the liquid, another proof that the Kelvin–Helmholtz mechanism is not involved in the primary instability.

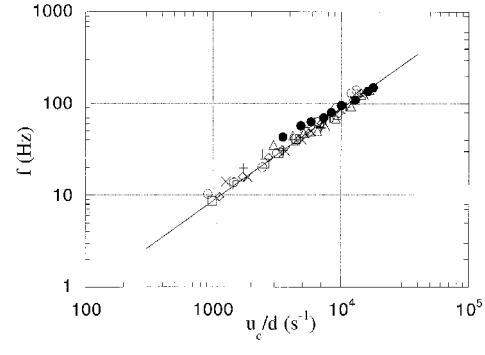

Fig. 4 Interface destabilization frequency f of the plane, two-phase shear-layer setup of Fig. 2b vs u_c/δ for different gas and liquid velocities. The proportionality [Eq. (13)] extends on more than one decade (from Raynal et al.[23]).

III. Flow Regimes: Potential Core Length and Recirculation Transition

A. Inner Potential Core Length

It is important to know at what distance from the injector outlet the central jet has been completely entrained by the inertial annular jet. By ''entrained'' we mean either mixed and diluted in the fast stream at the molecular level, or converted into disjointed and dispersed droplets. In the latter case this distance is usually referred to as the ''liquid intact length'' or ''breakup length.'' More generally, one might be interested in characterizing the whole concentration, or probability of presence field of the central slow phase at each location downstream of the injector outlet. Before this last issue is discussed we examine a simple argument to understand how the inner potential core length depends on the external parameters, i.e., u_1, u_2, ρ_1, and ρ_2.

The concept of entrainment velocity meets an interest when the local conversion processes occur at a scale smaller than the global extent of the surface at which the entrainment takes place. This condition is realized here because the instability wavelength λ is usually smaller than the inner potential core length itself (albeit not drastically smaller, see Rehab et al.[22]). One might thus use with some confidence the entrainment velocity [Eq. (4)] as a representative mean value along the entrainment surface to estimate its length. The last supplementary ingredient to achieve this goal is mass conservation, expressing that the net flow rate injected in the central jet has to cross the entrainment interface at the u_e rate. This approach was already used by Taylor[7] and has been commonly adopted since then in the context of airblast atomization.[12] Its use has also been successful to estimate the shape and extent of laminar diffusion flames[26] and turbulent diffusion flames.[27]

The mass balance for the inner entrained stream is written (Fig. 2)

$$\underbrace{\frac{\pi}{4} D_1^2 u_1}_{\text{inlet flux}} = \underbrace{\frac{\pi}{2} D_1 \left[\left(\frac{D_1}{2} \right)^2 + L^2 \right]^{1/2}}_{\text{entrainment surface}} \underbrace{u_e}_{\text{rate}} \tag{15}$$

if the mean surface is assumed to be a cone, and L is its height, and if u_e is constant up to L, i.e., $(D_2 - D_1)/D_1$ is sufficiently important.[28] The length L here is the inner potential core length. As long as $L >> D_1/2$, one expects

$$L/D_1 \approx u_1/u_e \tag{16}$$

The potential core length is in direct proportion to the inlet velocity u_1 (the more to be entrained, the longer it takes to complete it), and inversely proportional to the efficiency of the conversion rate u_e. According to the general form taken by u_e [see Eq. (4)], L is thus found to scale as

$$(L/D_1) \sim (u_1/u_2)(\rho_1/\rho_2)^{1/2} \sim M^{-1/2} \tag{17}$$

This scaling dependency was not, surprisingly, because of the universal form [Eq. (4)], derived by Caré and Ledoux,[12] and for a somewhat different application by Taylor[7] on the basis of a Kelvin–Helmholtz description of the primary instability. But the possible success of Eq. (17) in predicting L (it will show later that it actually succeeds), cannot be, as emphasized in Sec. II, considered as proof that the microscopic model of instability is well founded.

There is, however, a global mean quantity characterizing the spray-formation process that easily measurable is sensitive to the microscopic physics, namely the initial spray angle. Its tangent is given by the ratio of the entrainment velocity u_e to the group velocity of the unstable structures at the interface $u_c = \partial/\partial k(Re[\omega(k)])$

$$\tan \theta \sim u_e/u_c \tag{18}$$

In the reference frame of the liquid-gas interface, the spray angle is found to be proportional to the square root of the momentum ratio $\sqrt{M} = u_2/u_1(\rho_2/\rho_1)^{1/2}$, when the group velocity is essentially given by u_1, as for the pure Kelvin–Helmholtz mechanism [see Eq. (5) Refs. 12 and 29]. On the other hand, the spray angle with respect to the interface is constant, of the order of 45 deg in the boundary-layer-dominated regime for which $u_c \sim u_2(\rho_2/\rho_1)^{1/2} \sim u_e$ [see Eq. (14)]. In this latter case, the opening angle of the spray is thus expected to decrease in the reference frame of the laboratory when M is increased,[30] and this is because of the shortening of L. In this fixed frame it is readily shown that the angle is expected to depend on M as $(\pi/4) - \arctan(M^{1/2}/6)$.

The one-phase experiments (water–water jets) specifically established the structure of Eq. (17), extending its validity to the whole concentration field of the entrained phase.[6,22] These authors first showed that the prefactor in Eq. (17) is related to the proportionality coefficient between the entrainment velocity and the rms velocity u' in the outer turbulent mixing layer, $u' \approx \alpha u_2$, $\alpha \approx 0.17$,[31–33] and, to a minor extent, to the shape of the velocity profile of the central stream and pre-existing turbulence in the conveying tubes.[34] The potential core length was thus found to be

$$L/D_1 = A/M^{1/2}, \quad \text{with} \quad A = 6\text{–}8 \tag{19}$$

For coaxial injectors operating in practical conditions ($M \approx 10$), L is the order of a few i.d. D_1 units if the effects of the combustion heat release on the gas density are disregarded at this point. Very low-momentum ratios ($M < 1$) cause the inner jet to destabilize very slowly in a nearly passive environment, and in that case L/D_1 can be very large.[35,36] Extrapolating the preceding reasoning to the limit $M \to 0$ for an ambient medium at rest, the relevant shear velocity becomes u_1 and Eq. (19) becomes $L/D_1 \approx A(\rho_1/\rho_2)^{1/2}$, giving a liquid core the order of thousands of injection diameter D_1 for a water jet discharging in air at atmospheric pressure.[2,37,38,63]

Using planar cuts containing the axis of the jets and a quantitative laser-induced fluorescence technique, Rehab et al.[6] extracted the whole, two-dimensional concentration field (or probability of presence field) of a dye injected in the central jet (Fig. 5). Note that in homogeneous fields, the square root of the momentum ratio amounts to the velocity ratio $r_u = u_2/u_1$.

Figure 6a represents the mean concentration distributions C along the jet axis normalized by the initial mean concentration C_0 at the inner nozzle exit extracted from averaged images as in Fig. 5. It is observed that the mean normalized concentration is constant along the inner unmixed region and then decreases in the mixing zone where the two streams meet on the axis. The unmixed zone corresponds to the inner potential core. The dilution length L_s is the distance from the outlet to reach a given dilution level C_s/C_0 on the axis. Figure 6c represents the evolutions of L_s as a function of the velocity ratio r_u for three values of the dilution level $C_s/C_0 = 1$, 0.9, and 0.5. L_s follows a law similar to Eq. (19), i.e., $L_s/D_1 = A_s/r_u$, independently of the dilution level, the constant A_s being an increasing function of C_s/C_0. It is found that $L_s/D_1 = 12/r_u$ for $C_s/C_0 = 0.5$, whereas for $C_s/C_0 = 1$, $L_s/D_1 = 6/r_u$. Also in Fig. 6 are the results of the inner potential cone length obtained from velocity field measurements in the same experiments.[22] These coincide with the dilution length corresponding to $C_s/C_0 = 0.9$.

Consistent with the fact that the dilution lengths are inversely proportional to r_u, whatever C_s/C_0 may be, the mean concentration profiles of Fig. 6a display a perfect superposition when the downstream coordinate is rescaled according to $(x/D_1)r_u$, thus confirming the importance of the velocity ratio $r_u = \sqrt{M}$ as the key parameter (see Fig. 6b and Ref. 39). The dilution length evolution laws again reflect mass conservation. Showing that any isoconcentration surface is crossed by the inlet dye flux, one sees that $L_s/D_1 \approx (C_0/C_s)(8/r_u)$ is in agreement with Fig. 6c. At large distances x/D_1 from the end of

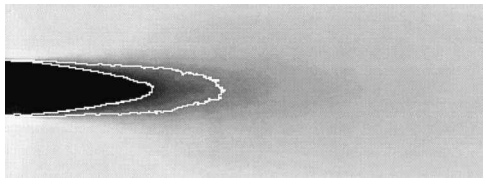

Fig. 5 Averaged concentration fields of a dye injected in the central jet for $r_u = 3$ ($M = 9$). The white contours correspond to the dilution levels $C_s/C_0 = 0.5$ and 0.9.

the potential core, the normalized concentration decays as $(x/D_1)^{-1}$, as dictated by the global mass conservation in the far field of a round jet.

This far-field spatial dependency is also recovered by Carreau et al.,[40] using a fiber-optics probe to measure the liquid fraction on temporal traces of punctual measurements in a two-phase experiment. In this interesting investigation, performed on the MASCOTTE test facility at ONERA, these authors varied the intrinsic density of the gas by a factor of 10 (from helium to argon) at atmospheric pressure. Keeping the momentum ratio M about 6.6 and the velocity of the liquid u_1 constant, they observed a systematic shortening of the liquid fraction fields as ρ_2/ρ_1 was increased, inducing an apparent, intrinsic effect of the density ratio on the breakup length at fixed M.

The liquid fraction or probability of presence of the liquid is estimated in the experiments of Carreau et al. from the number and length of the intercepts of the tip of the probe with the liquid packets detected by a double threshold level technique. As emphasized by Cartellier,[41] this technique has to be used with caution because due to the unavoidable limited spatial resolution of the probe, it leads to an underestimation of the presence of liquid by discarding the small, but numerous droplets. As shown in Sec. IV the typical droplet size resulting from the primary instability is expected to get increasingly smaller as ρ_2/ρ_1 is increased for fixed M and u_1. When the liquid fraction is computed from a droplet-detection technique, it thus results in an underestimation bias that is increasingly pronounced as the droplet size gets smaller compared to the detection scale limit of the probe. This might possibly explain the systematic bending of the liquid-fraction profiles in the experiments of Carreau et al.,[40] which, symmetrically, can be interpreted as an interesting, though indirect, striking proof that the droplet size of the primary breakup is actually a decreasing function of ρ_2/ρ_1, for fixed momentum ratio (Sec. IV).

Correlations for the breakup length in two-phase conditions usually involve an aerodynamic Weber number and the liquid-phase Reynolds number.[3,42,43] These parameters are, in fact, introduced to make the gas and liquid velocities nondimensional in experiments where neither the surface tension, nor the viscosity of the liquid have been varied.[44] Reinterpreted in terms of momentum ratio M, these correlations present grosso modo a good agreement with Eq. (19), in absolute values and in law.[38,45] The independence of L on surface tension and liquid viscosity has been checked in the plane mixing-layer configuration of Fig. 2b.

The apparent dependency on M is found[43,46] to be somewhat weaker than for homogeneous conditions and it seems to involve a dependency closer to $M^{-0.33}$. It is not perfectly clear whether the momentum ratio should be the only scaling parameter in that case. In this discrepancy there is an interesting question that may be indicative of when the mass ratio

$$m = \frac{\rho_1 u_1}{\rho_2 u_2} \frac{D_1^2}{D_2^2 - D_1^2}$$

is not negligibly small as it is for a large density ratio ρ_1/ρ_2; it might come into play in the scaling relations, as suggested in Lasheras et al.[24] It could also be that the wavelength of the primary instability $\lambda \sim \delta(\rho_1/\rho_2)^{1/2}$ becomes of the same order of magnitude as L for a large-density ratio. In that case the entrainment velocity u_e cannot any longer be considered as constant along the whole entrainment length. The initiation distance of the entrainment corresponds to about one wavelength downstream of the injector outlet, so that writing

$$u_e \approx \frac{u_{e\infty}}{1 + a(\lambda/L)}$$

where $u_{e\infty} \sim u_2(\rho_2/\rho_1)^{1/2}$, the liquid intact length is found to scale as $L/D_1 \approx 6/M^{1/2} + a\lambda/D_1$ to leading order in λ/D_1, with $a \approx 1/4$.

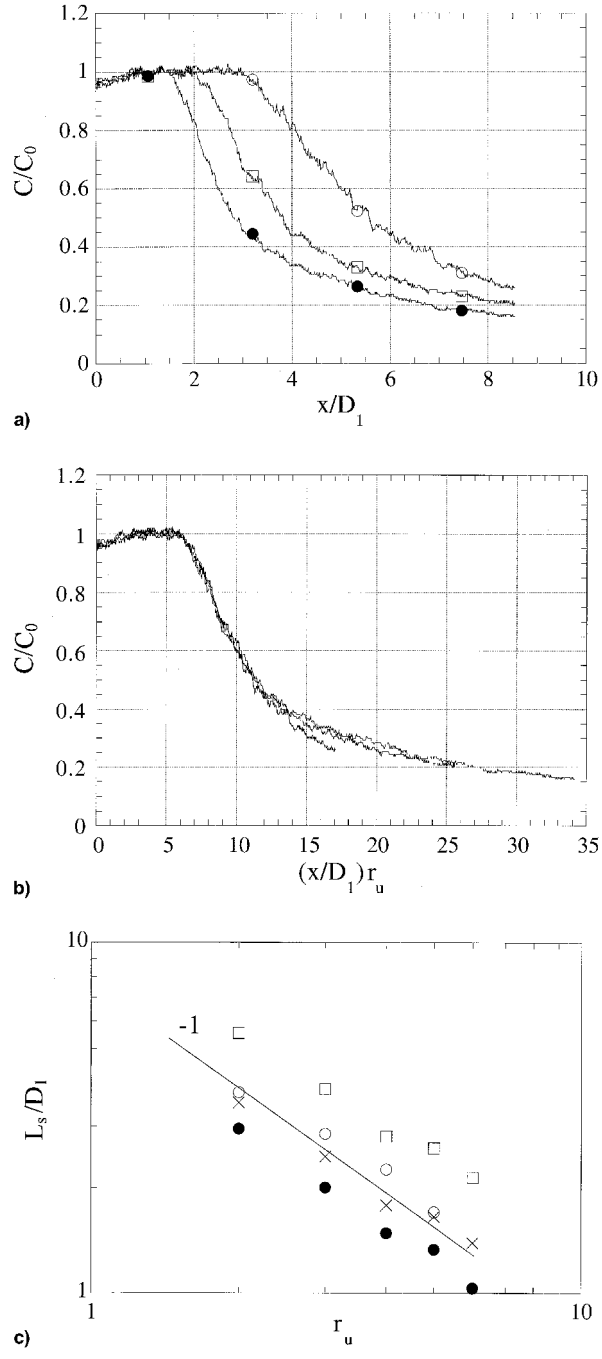

Fig. 6 a) Mean concentration evolutions along the axis (adapted from Rehab et al.[6]) ○, $r_u = 2$; □, $r_u = 3$; ●, $r_u = 4$. b) Collapse of the mean concentration profiles of part a) by the scaled space variable $(x/D_1)r_u$. c) Dependence of the dilution lengths L_s on the velocity ratio r_u. ●, $C_s/C_0 = 1$; ×, $C_s/C_0 = 0.9$; □, $C_s/C_0 = 0.5$; ○, determined from the velocity field.

B. Recirculation Transition

The entrainment process is accompanied by a depression in the entrainment region of the order of $\Delta P \sim \rho_2 u_2^2$ [see Eq. (2)]. As long as the incident kinetic pressure of the central jet $\rho_1 u_1^2$ is high enough to overcome ΔP, the flow regime is characterized by an inner potential cone peeled off by turbulent mixing layers as described in Sec. III.A. However, when the entrainment is so intense that ΔP is larger than the incident kinetic pressure, a transition to a recirculating regime occurs, where the central potential cone is truncated by a reverse flow directed from the outer jet to the inner one, leaving in its place a wake-like, recirculation bubble.[22,28] The critical momentum ratio M_c at which this transition occurs is obtained by equating ΔP with $\rho_1 u_1^2$, remembering that $u' \approx \alpha u_2$ and $\alpha = 0.17$

$$\alpha^2 \rho_2 u_2^2 = \rho_1 u_1^2 \tag{20a}$$

that is

$$M_c \approx (1/\alpha^2) \approx 35 \tag{20b}$$

An extension of this result to a centrifugal force has been proposed by Hopfinger and Lasheras.[47] Above the critical momentum ratio [Eq. (20)], the size of the recirculation bubble gradually increases, reaching a size of the order of D_1 when $M \to \infty$.

A common feature of unstable, recirculating flows is their ability to sustain oscillations. Villermaux et al.[28] and Rehab et al.[22] precisely documented the low-frequency, precessing mode that is distinct from the jet-preferred mode that appears for $M > M_c$, and they explained how the low frequency is the result of the slow recirculation motion.

The recirculating regime also presents the capability of an efficient and precocious mixing between the streams in the vicinity of the injectors outlet (Fig. 7). A high-Schmidt-number (ratio of the vorticity to the mass diffusivities) dye injected in the outer jet exhibits an intensity of segregation in the bubble about 10 times smaller than at its frontiers.[6] The reason is that in this regime, the residence time of the outer stream, incorporated in the bubble is of the order of the mixing time D_1/u'; D_1 being an order of magnitude of the recirculation bubble size, and u' the rms velocity of the turbulent mixing layers. This residence time is much longer than the transit time D_1/u_2 on the same distance; therefore leading an efficient homogenization in this recirculation region (Fig. 8).

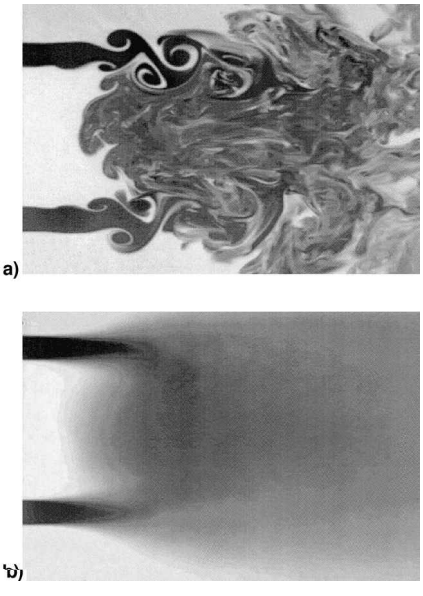

Fig. 7 Flow pattern beyond the recirculation transition, $r_u = 15$ ($M = 225$): a) instantaneous view and b) averaged concentration field.

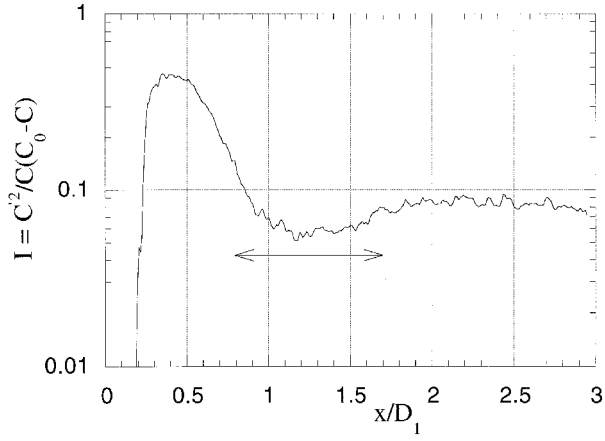

Fig. 8 Distribution of intensity of segregation $I = C'^2/C(C_0 - C)$ along the jet's axis for $r_u = 15$. C' stands for the local rms fluctuation of concentration, and C is the local mean concentration. The arrows indicate the width of the recirculation zone (from Rehab et al.[6]).

Actual rocket engines usually operate at a momentum ratio of the order of 10, smaller than critical. Increasing M to critical or supercritical momentum ratio could probably yield shortened combustion chambers.

IV. Fine Structure of the Mixture and Spray Formation

This paper does not imply that surface tension plays no role in atomization, the converse is obviously true. Once unstable structures have been produced at the interface by the primary shear instability, their fate is to be further stretched and elongated by the high-speed stream, possibly to undergo secondary instabilities before being, in one phase flows, mixed at a molecular scale (see, e.g., Fig. 1). The initial wavelength of the instability is independent of capillary effects, but surface tension, when it exists, opposes the scale-reduction process by stretching to ultimately involve a capillary instability that fixes the primary droplet size.

In this section a possible route to droplet formation is discussed, where the initial scale of the disturbances λ given by Eq. (11b) happens to play a crucial role.

A. Rim Recession and Capillary Instability

Surface tension mainly plays a stabilizing role in nature. It stabilizes shear as in the Kelvin–Helmholtz scheme, but also an interface subjected to a gravitational destabilization as in the Rayleigh–Taylor problem. The only situation where surface tension is the source of the instability is when a liquid lump has an initial shape close to a long cylinder, as for a jet. In that case, following an argument from Plateau,[48] a modulation of the radius of the jet along the axis causes its surface to decrease (at a constant volume) and, therefore, its surface energy, thus favoring the perturbed state for all wavelengths longer than the perimeter of the jet. The full instability problem including the dynamics was solved by Rayleigh.[49] The effect is opposite when the liquid initially has the shape of a flat sheet, because any modulation of its thickness causes its surface energy to increase. For droplets to form from an initially compact liquid volume, the liquid must thus conform into a cylindrical shape, even transitorily.

The paradox is that shear instabilities, producing two-dimensional rolling-up billows tend to form sheets instead of jets or fingers, even when the streamwise instabilities (Figs. 1a and 1b) have developed. But these are bounded sheets, with an ending rim, whose dynamics solves the paradox (Fig. 9). The phenomenon is particularly well illustrated by the splashing

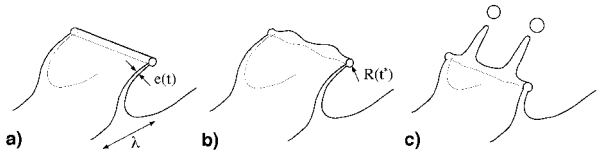

Fig. 9 Sketch of the rim destabilization and droplet formation process: a) thinning of the liquid sheet of initial transverse size of the order of λ and rim recession; b) capillary, Rayleigh-type destabilization of the rim; and c) formation of fingers with a spacing given by the capillary instability wavelength and drop formation by the Rayleigh capillary instability of the fingers.

experiments of Worthington[50] (see also Yarin and Weiss[51]), and by the pictures of spray production from flat sheets of Dorman[52] and Taylor,[53] and the three-dimensional simulations of Zaleski et al.[54] performed in the precise context of shear instabilities and which, in addition, point out the important role of the spanwise perturbations on the earliness of drop breakup by finger formation.

Let e be the thickness of the liquid sheet at a given instant of time. Because of the Laplace–Young force that is inversely proportional to the radius of curvature of the rim ($\approx e/2$), the rim tends to recess, and it is easily shown that it does so at a constant velocity v such that[53]

$$v = (2\sigma/\rho_1 e)^{1/2} \tag{21}$$

Then the rim, agglomerating liquid during its recession, progressively takes the shape of a cylinder attached to the liquid sheet that feeds it, and whose radius $R \sim (evt)^{1/2}$ increases in time.

Now, according to the inviscid Plateau–Rayleigh result, the cylinder is unstable to a capillary instability, with a maximal growth rate equal to

$$r_{\text{cap}} = 0.34(\sigma/\rho_1 R^3)^{1/2} \tag{22a}$$

corresponding to a wavelength $2\pi/k_m$ such that

$$k_m R \approx 0.69 \tag{22b}$$

The radius is itself a function of time, and one can show that as soon as

$$\frac{1}{R}\frac{\mathrm{d}R}{\mathrm{d}t} < r_{\text{cap}} \tag{23}$$

the capillary instability sets in, with a wavelength [Eq. (22b)] based on the current value of the rim radius R. From the instant of formation of the sheet at thickness e, the time needed to accomplish the condition [Eq. (23)] scales as $t_* \sim e/v$, providing, via the Rayleigh instability, a droplet radius proportional to e

$$R(t_*) \sim e \tag{24}$$

A possible bag-type breakup that is associated with the formation of a very thin sheet whose disintegration is caused by Van der Waals forces, has not been considered here. This phenomenon produces very small droplets,[55] carrying a small fraction of the initial liquid volume.

B. Stretching-Assisted Sheet Formation and Droplet Size

The initial quasi-two-dimensional interface disturbances, of typical size $\lambda \sim \delta(\rho_1/\rho_2)^{1/2}$, are further stretched in the high-speed gas stream, increasing in length and decreasing in thickness. The question is now to determine how e is related to λ and to the relevant stretching rate. This is not an obvious question. There are, a priori, two velocity scales in the problem, namely u_2 and $u_e \sim u_2(\rho_2/\rho_1)^{1/2}$, which might differ appreciably. It is readily shown that the time τ needed to accelerate a liquid lump of size λ to the high-speed velocity is larger than its formation time r^{-1}, i.e., $r\tau \approx 1/C_D(\rho_1/\rho_2)^{1/2}$, where $C_D \approx 1$ and, as can be seen from Eq. (25), larger than the breakup time t_*, i.e., $rt_* \approx We^{1/5}(\rho_1/\rho_2)^{1/10}$. One can thus assume that the disturbances keep their initial peeling-off velocity u_e while they are stretched from the interface, and that the rate of stretch amounts to $u_e/\lambda = r = (u_2/\delta)(\rho_2/\rho_1)$. The current transverse thickness decays as $e(t) \sim \lambda/rt$, and from $t_* \sim e/v$ and $v \sim (\sigma/\rho_1 e)^{1/2}$ one derives the thickness of the sheet $e(t_*)$ at the breakup time

$$e(t_*) \sim \frac{\lambda}{rt_*} = \frac{\lambda}{(rt_0)^{2/5}} \tag{25a}$$

with

$$t_0 = \frac{\lambda}{(\sigma/\rho_1\lambda)^{1/2}} \tag{25b}$$

Note that $e(t_*)/\lambda \sim We^{-1/5}(\rho_1/\rho_2)^{-1/10}$; the thickness of the sheet is actually smaller than the initial wavelength λ.

The droplet radius is therefore expected to scale as [Eq. (24)]

$$\frac{R}{\lambda} \sim \left[\frac{u_e}{\lambda}\frac{\lambda}{(\sigma/\rho_1\lambda)^{1/2}}\right]^{-2/5} \tag{26a}$$

that is

$$\frac{R}{\delta} \sim We^{-1/5}\left(\frac{\rho_1}{\rho_2}\right)^{2/5} \tag{26b}$$

with δ being the thickness of the fast-stream-velocity profile at the location of droplet formation. The preceding relation constitutes the central result of this section and incorporates several predictions that deserve a separate discussion.

1. *Effect of Linear Scale on Drop Size*

Up to now δ has been conserved as the characteristic thickness of the fast-side-velocity profile along the whole entrainment distance L. This is obviously an oversimplification because the thickness of the gas layer clearly increases as the instability develops (see, e.g., Fig. 1). This caricature does not affect the estimation of the entrainment velocity at all because as shown in Sec. II.A u_e is a scale invariant quantity: A slight renormalization of the wavelength λ to the increased thickness of the gas layer does not therefore affect the entrainment rate.

Let $\Delta(x)$ be the current gas-layer thickness at distance x from the injector's outlet: $\Delta(0) = \delta$ and we will need to compute $\Delta(L)$. At very large distances x, when the shear layer has had time enough to reach the fully developed mixing layer regime, $\Delta(x)$[33] follows a linear dependency on x. This is readily justified by making use of a turbulent diffusivity $\nu_t \sim u'\Delta(x)$, with u' being the rms velocity in the layer. Then, with $\Delta(x) \sim \sqrt{\nu_t x/u_2}$, one arrives at $\Delta(x) \sim (u'/u_2)x$.

At intermediate distances, however, because of the slow entrainment process (increasingly slow as ρ_1/ρ_2 is larger), one might expect the relevant diffusivity ν_t to depend on the size and velocity of the structures mediating the entrainment, i.e., $\nu_t \sim u_e\lambda \sim u_2\delta$; then, from $\Delta(x) \sim \sqrt{\nu_t x/u_2}$, one gets

$$\Delta(x) \sim (\delta x)^{1/2} \tag{27a}$$

that is

$$\Delta(L) \sim (\delta D_1)^{1/2} M^{-1/4} \tag{27b}$$

The size of the liquid lumps peeled off from the interface gets larger as one approaches the end of the inner potential core, the thickness $\Delta(L)$ being appreciably larger than δ. This is clearly apparent in Fig. 1. A similar observation, consistent with the scaling law [Eq. (27a)] has been made by Wu et al.[56]

Together with the general form of the droplet size [Eq. (26b)], where δ has been replaced by $\Delta(L)$ given by Eq. (27b), one finds

$$R \sim \frac{(\delta D_1)^{2/5}}{(\rho_2 u_2^2/\sigma)^{1/5} M^{1/5}} \left(\frac{\rho_1}{\rho_2}\right)^{2/5} \tag{28}$$

Before discussing other scaling dependencies, let us first comment on the drop-size R dependency on the linear scales δ and D_1. Equation (28) suggests $R \sim (\delta D_1)^{2/5}$. In this result there is an interesting consistency with yet unexplained results, where on different setups a relation of the form SMD $\sim$ (initial thickness of the liquid)$^{0.38-0.4}$ has been repeatedly found.[3,57,58] The SMD (Sauter mean diameter) is a weighted average of the full probability density function (PDF) of the droplet sizes that privileges the large excursion wing of the PDF. This corresponds to the biggest droplets formed near the end of the potential core so that Eq. (27b) is actually the appropriate estimate to compute Eq. (28). We thus claim that the apparent exponent 0.38–0.4 indeed means 2/5, and we also note that this dependency should also hold when the initial shear layer gas thickness δ is varied.

2. *Effect of the Gas Density at Fixed Momentum Ratio on Drop Size*

It is not possible, for a given inlet flow rate of liquid, to independently set the liquid intact length L and the droplet size R. Consider, for example, an experiment, as those of Carreau et al.,[40] where the liquid velocity u_1 and M are maintained constant when the density of the gas ρ_2, i.e., the nature of the gas or the pressure in the combustion chamber, is varied. In that particular situation, the liquid intact length is essentially constant (see Sec. III.A) and because u_1 is constant, $\rho_2 u_2^2$ is constant as well. The droplet size scales according to Eq. (28), as $R \sim \delta^{2/5}\rho_2^{-2/5}$. If the exit conditions in the gas phase are laminar $\delta \sim (D_2 - D_1)Re^{-1/2} \sim (\rho_2 u_2)^{-1/2}$, one has $R \sim \rho_2^{-3/10}$. If the exit conditions are turbulent, δ identifies to the viscous sublayer thickness of the turbulent gas boundary layer at the periphery of the inner tube $\nu_2/u_2 \sim (\rho_2 u_2)^{-1}$ and, thus, $R \sim \rho_2^{-3/5}$. In both cases, the typical drop size decreases when ρ_2 is increased, meaning that the whole PDF of droplet is shifted toward the small sizes. This fact, as mentioned in Sec. III.A, might explain the apparent anomalous decrease of the liquid fraction by increasing ρ_2 when a spurious cutoff is introduced on the PDF integration by the probe resolution. Lengths of constant liquid fraction, i.e., 0.5, were found to decrease as $(\rho_2/\rho_1)^{-0.32}$ at fixed M by Carreau et al.[40] in experiments using a 90-μm-thick fiber-optics probe (see Sec. III.A). The SMD, measured independently by an optical, nonintrusive, resolvant method (PDPA) were found to be of the order of 75 to 40 μm.

3. *Gas Velocity Dependency of Drop Size*

Again from Eq. (28), the dependency of the droplet size R on the gas velocity u_2 can be derived, with the remaining control variables (u_1, ρ_1, ρ_2) constantly maintained.

For laminar-exit conditions at the gas-tube outlet [$\delta \sim (D_2 - D_1)Re^{-1/2} \sim u_2^{-1/2}$], one finds that $R \sim u_2^{-1}$. For turbulent exit conditions ($\delta \sim \nu_2/u_2$), one gets $R \sim u_2^{-6/5}$. It is interesting to note that this scaling dependency is exactly the same as the one derived by Kolmogorov[59] for the droplet equilibrium diameter in a fully developed turbulent flow (see Faeth et al.[2]). It is, however, derived here from an absolutely nonturbulent scenario, invoking neither any cascade process, nor any preexisting hierarchy of scales in the flow, but solely primary shear and capillary instability arguments.

C. Role of the Liquid Viscosity

The scenario of drop formation leading to the drop size [Eq. (28)] assumes that the initial transverse size of the liquid sheet is essentially given by the primary shear instability wavelength λ, and we have described how stretching induced thinning of the sheet leads to drop breakup.

One might think about a completely different mechanism for the initial formation of the sheet. As the liquid surface gets corrugated by the development of the instability, the gas flow separates downstream of the crests, isolating a low velocity, recirculating pocket in the manner of the separated bubble downstream of a backward-facing step.[60] In the reference frame of the interface disturbances [which propagate at a velocity u_c, see Eq. (14)], the liquid interface is thus progressively reaccelerated from a separated region to the next interface crest, at a downstream distance λ apart. One readily shows that the interfacial velocity u_i of the liquid at the crests writes approximately $u_i \sim \omega_0\sqrt{\nu_1\lambda/u_i}$, where $\omega_0 = (\eta_2/\eta_1)(u_2/\delta)$, by continuity of the stress at the interface. The thickness of the vorticity layer in the liquid is then $\delta_1 \sim \sqrt{\nu_1\lambda/u_i}$. This viscous layer will be peeled off from the interface if the viscous stress $1\eta_1(u_i/\delta_1)$ exceeds the Laplace–Young recessing constraint σ/δ_1, that is to say if

$$Ca = \eta_1 u_i/\sigma >> 1 \tag{29}$$

With the preceding estimate for the interfacial velocity $u_i \sim u_2 Re^{-1/3}(\nu_2/\nu_1)^{1/3}(\rho_2/\rho_1)^{1/2} << u_2$, it is seen that the capillary number $Ca \sim (We/Re^{4/3})(\nu_1/\nu_2)^{2/3}(\rho_1/\rho_2)^{1/2}$ is, in practical conditions and because of its Reynolds-number dependency, smaller than unity. This scenario, somewhat related to a mechanism proposed by Taylor[61] and Wu et al.[56] in a different context, will most likely not occur.

We must emphasize that the droplet size relations derived in this section are to be understood as mean, typical estimates, representative of the relevant physical quantities and scaling relations. A salient feature of airblast atomization processes is their property to produce broad PDFs of droplet sizes, with a nonvanishing small proportion of big lumps that remain in the spray (and may even cross the flame front, see Gicquel et al.[62]). The secondary breakup mechanisms and the role played by the far-field gas jet turbulence in that case have also not been discussed (see, e.g., Lasheras et al.[24]). The understanding of the full shape of the PDF if different physical processes happen to cooperate to its global form would be welcome.

V. Summary and Conclusions

The point of view demonstrated in this paper is that the global entrainment rate from the inner, slow dense jet to the outer, annular fast light stream, and also the primary drop formation in liquid-gas coaxial jets can be understood on the basis of the primary shear instability between the phases. It is shown that the shape of the velocity profile at the outer injector lip, and precisely its vorticity thickness δ is of primary importance to set the growth rate $r \sim (u_2/\delta)(\rho_2/\rho_1)$ of the instability and its preferred wavelength $\lambda \sim \delta(\rho_1/\rho_2)^{1/2}$, where ρ_1/ρ_2 is the ratio of the dense to the light phase densities. The scale invariant entrainment velocity $u_e \approx r\lambda \sim u_2(\rho_2/\rho_1)^{1/2}$ gives rise, via mass conservation, to an inner potential core length (liquid intact length) L of the form

$$L/D_1 = 6/M^{1/2}$$

where D_1 is the i.d. and $M = \rho_2 u_2^2/\rho_1 u_1^2$ is the momentum ratio between the phases. L is independent of liquid viscosity and surface tension. For $M > M_c \approx 35$, a transition to a recirculation flow occurs, whose efficient mixing properties are quantified.

When the inner jet is liquid, we have suggested that the primary drop size R results from the capillary instability of the

rim at the edge of the sheets formed from the initial shear instability disturbances and stretched in the fast gas stream. Accounting for the thinning rate of the liquid sheet in the description of the breakup process of the rim, it was further anticipated that the drop radius scales as

$$\frac{R}{\delta} \sim \frac{(D_1/\delta)^{2/5}}{We^{1/5}M^{1/5}} \left(\frac{\rho_1}{\rho_2}\right)^{2/5}$$

if $We = \rho_2 u_2^2 \delta/\sigma$ is the Weber number based on the initial gas vorticity thickness δ. According to this scenario, the liquid viscosity is not expected to participate in the determination of the drop size in most practical conditions, including those prevailing in rocket engines.

The discussion has been supplemented with several experimental facts, both in one- and two-phase flows, and the connection with known results in the field of airblast atomization has been made.

Acknowledgments

This work is part of the GdR "Combustion dans les moteurs de fusée," Centre National d'Études Spatiàles–Centre National de la Recherche Scientifique–Société Européenne de Propulsion–Office National des Etudes et de Recherches Aérospatiales and was supported by a SEP Grant under Contract 910023. The constant interaction with E. J. Hopfinger and our common Ph.D. students L. Raynal and H. Rehab, whose work is broadly reported in this paper is appreciated. J. L. Carreau, P. Gicquel, E. Porcheron, and L. Vingert are gratefully acknowledged for sharing their results. Stimulating discussions with C. Clanet and S. Zaleski on the drop formation problem, and with A. Cartellier and J. C. Lasheras on related topics were very helpful.

References

[1]Beér, J. M., and Chigier, N. A., *Combustion Aerodynamics*, Applied Science Publishers, Ltd., London, 1972.

[2]Faeth, G. M., Hsiang, L. P., and Wu, P. K., "Structure and Breakup Properties of Sprays," *International Journal of Multiphase Flow*, Vol. 21, Suppl., 1991, pp. 99–127.

[3]Lefebvre, A. H., *Atomization and Sprays*, Hemisphere, Taylor and Francis, 1989.

[4]Vingert, L., Gicquel, P., Lourme, D., and Ménoret, L., *Coaxial Injector Atomization*, Progress in Astronautics and Aeronautics, AIAA, New York, Vol. 169, 1994, pp. 145–157.

[5]Ledoux, M., Caré, I., Micci, M., Glogowski, M., Vingert, L., and Gicquel, P., *Atomization in Coaxial-Jet Injectors*, Progress in Astronautics and Aeronautics (to be published) 1998.

[6]Rehab, H., Villermaux, E., and Hopfinger, E. J., "Flow Regimes and Mixing in the Near Field of Large Velocity Ratio Coaxial Jets, *Proceedings of the 11th Symposium on Turbulent Shear Flows* (Grenoble, France), 1997, pp. 7–10.

[7]Taylor, G. I., "Generation of Ripples by Wind Blowing over a Viscous Fluid," *Collected Works of G. I. Taylor*, edited by G. K. Batchelor, 1940, Paper 25.

[8]von Helmholtz, H., "Über discontinuirliche Flüssigkeits bewegungen," *Monats. Königl. Preuss. Akad. Wiss. Berlin*, Vol. 23, 1868, pp. 215–228; also "On Discontinuous Movements of Fluids," *Philosophical Magazine*, Vol. 36, No. 4, 1868, pp. 337–346.

[9]Kelvin, Lord, "Hydrokinetic Solutions and Observations." *Philosophical Magazine*, Vol. 42, No. 4, 1871, pp. 362–377.

[10]Chandrasekhar, S., *Hydrodynamic and Hydromagnetic Stability*, Clarendon, Oxford, England, UK, 1961.

[11]Landau, L. D., and Lifchitz, E. M., *Mécanique des Fluides*, Mir, Moscow, 1989.

[12]Caré, I., and Ledoux, M., "Study of an Airblast Coaxial Atomizer. Experiments and Modelization," *Proceedings of the ICLASS 91 Conference* (Gaithersburg, MD), 1991, pp. 763–770 (Paper 85).

[13]Squire, H. B., "Investigation of the Stability of a Moving Liquid Film," *British Journal of Applied Physics*, Vol. 4, 1953, pp. 167–169.

[14]Rayleigh, Lord, "On the Stability, or Instability, of Certain Fluid Motions," *Proceedings of the London Mathematical Society*, Vol. 11, 1880, pp. 57–70.

[15]Esch, R. E., "The Instability of a Shear Layer Between Two Parallel Streams," *Journal of Fluid Mechanics*, Vol. 3, 1957, pp. 289–303.

[16]Monkewitz, P., and Huerre, P., "Influence of the Velocity Ratio on the Spatial Instability of Mixing Layers," *Physics of Fluids*, Vol. 25, No. 7, 1982, pp. 1137–1143.

[17]Pouliquen, O., Chomaz, J. M., and Huerre, P., "Propagating Holmboe Waves at the Interface Between Two Immiscible Fluids," *Journal of Fluid Mechanics*, Vol. 266, 1994, pp. 277–302.

[18]Li, J., and Zaleski, S., "Direct Simulation of Spray Formation," *Proceedings of the ICLASS 97 Conference* (Seoul, Republic of Korea), Begell House, New York, 1997, pp. 812–816.

[19]Villermaux, E., "Auto-Oscillation et Mélange dans les Écoulements Recirculants," Ph.D. Dissertation, Univ. Pierre et Marie Curie, Paris VI, 1993.

[20]Villermaux, E., "On the Role of Viscosity in Shear Instabilities," *Physics of Fluids*, Vol. 10, No. 2, 1998, pp. 368–373.

[21]Schlichting, H., *Boundary Layer Theory*, McGraw–Hill, New York, 1987.

[22]Rehab, H., Villermaux, E., and Hopfinger, E. J., "Flow Regimes of Large Velocity Ratio Coaxial Jets," *Journal of Fluid Mechanics*, Vol. 345, 1997, pp. 357–381.

[23]Raynal, L., Villermaux, E., Lasheras, J. C., and Hopfinger, E. J., "Primary Instability in Liquid-Gas Shear Layers," *Proceedings of the 11th Symposium on Turbulent Shear Flows* (Grenoble, France), 1997, pp. 1–4.

[24]Lasheras, J. C., Villermaux, E., and Hopfinger, E. J., "Break-Up and Atomization of a Round Jet by a High Speed Annular Air Jet," *Journal of Fluid Mechanics*, Vol. 357, 1998, pp. 351–379.

[25]Bernal, L. P., and Roshko, A., "Streamwise Vortex Structure in Plane Mixing Layers," *Journal of Fluid Mechanics*, Vol. 170, 1986, pp. 499–525.

[26]Villermaux, E., and Durox, D., "On the Physics of Jet Diffusion Flames," *Combustion Science and Technology*, Vol. 84, 1992, pp. 279–294.

[27]Villermaux, E., "Fast Bimolecular Reactions in High Reynolds Number Turbulence: Structure of the Reactive Interface and Surface of Reaction," *Advances in Turbulence V*, edited by R. Benzi, Kluwer, Dordrecht, The Netherlands, 1995, pp. 529–533.

[28]Villermaux, E., Rehab, H., and Hopfinger, E. J., "Breakup Regimes and Self-Sustained Pulsations in Coaxial Jets," *Meccanica*, Vol. 29, 1994, pp. 393–401.

[29]Reitz, R. D., and Bracco, F. V., "Mechanism of Atomization of a Liquid Jet," *Physics of Fluids*, Vol. 25, No. 10, 1982, pp. 1730–1742.

[30]Mansour, A., and Chiguier, N., "Dynamic Behavior of Liquid Sheets," *Physics of Fluids A: General Physics*, Vol. 3, No. 12, 1991, pp. 2971–2980.

[31]Hill, B. J., "Measurement of Local Entrainment Rate in the Initial Region of Axisymmetric Turbulent Air Jets," *Journal of Fluid Mechanics*, Vol. 51, No. 4, 1972, pp. 773–779.

[32]Pitts, W. M., "Effect of Global Density Ratio on the Centerline Mixing Behavior of Axisymmetric Turbulent Jets," *Experiments in Fluids*, Vol. 11, 1991, pp. 125–136.

[33]Brown, G. L., and Roshko, A., "On Density Effects and Large Scale Structures in Turbulent Mixing Layers," *Journal of Fluid Mechanics*, Vol. 64, No. 4, 1974, pp. 775–815.

[34]Rehab, H., Villermaux, E., and Hopfinger, E. J., "Geometrical Effects on the Near-Field Flow Structure of Coaxial Jets," *AIAA Journal*, Vol. 35, No. 5, 1998, pp. 867–869.

[35]Mayer, W., and Tamura, H., "Flow Visualization of the Supercritical Propellant Injection in a Firing LOX/GH2 Rocket Engine," AIAA Paper 95-2433, 1995.

[36]Schik, A., and Krülle, G., "Investigation of Supercritical Coaxial Injection in H2/O2 Rocket Engines," *Proceedings of the Conference on Propulsive Flows in Space Transportation Systems* (Bordeaux, France), 1995, pp. 118–125.

[37]Hoyt, J. W., and Taylor, J. J., "Waves on Water Jets," *Journal of Fluid Mechanics*, Vol. 83, 1977, pp. 119–127.

[38]Chehroudi, B., Onuma, Y., Chen, S. H., and Bracco, F. V., "On the Intact Core of Full-Cone Sprays," Society of Automotive Engineers Paper 850126, 1985.

[39]Colin, P., and Stepowski, D., "The Liquid Volume Fraction and Its PDF in the Near Development Field of a Spray," *Proceedings of the 13th ILASS Conference* (Florence, Italy), 1997, pp. 389–394.

[40]Carreau, J. L., Porcheron, E., Le Visage, D., Prevost, L., and Roger, F., "Liquid Core Characterisation of Coaxial Liquid Oxygen/Inert Gas Jets," *Proceedings of the ICLASS 97 Conference* (Seoul, Republic of Korea), Begell House, New York, 1997, pp. 561–565.

[41]Cartellier, A., "Optical Probes for Local Void Fraction Measurements: Characterisation of Performance." *Review of Scientific Instru-*

ments, Vol. 61, No. 2, 1990, pp. 874–894.
[42]Arai, T., and Hashimoto, H., "Disintegration of a Thin Liquid Sheet in a Cocurrent Gas Stream," *Proceedings of the ICLASS 85 Conference* (London), VI.B.1, (1), 1985.
[43]Eroglu, H., Chigier, N., and Farago, Z., "Coaxial Atomizer Liquid Intact Length," *Physics of Fluids*, Vol. 3, No. 2, 1991, pp. 303–313.
[44]Carreau, J. L., Monoté, G., Le Visage, D., and Roger, F., "Atomization Characterization of an Assisted Injector," *Proceedings of the ASME Winter Annual Meeting Spray Symposium* (New Orleans, LA), 1993, pp. 51–58.
[45]Arai, M., Shimizu, M., and Hiroyasu, H., "Breakup Length and Spray Angle of High Speed Jets," *Proceedings of the ICLASS 85 Conference* (London), I.B.4, (1), 1985.
[46]Engelbert, C., Hardalupas, Y., and Whitelaw, J. H., "Breakup Phenomena in Coaxial Airblast Atomizers," *Proceedings of the Royal Society of London*, Vol. 451, 1995, pp. 189–229.
[47]Hopfinger, E. J., and Lasheras, J. C., "Explosive Breakup of a Liquid Jet by a Swirling Coaxial Gas Jet," *Physics of Fluids*, Vol. 8, No. 7, 1996, pp. 1696–1701.
[48]Plateau, J., *Statique Experimentale et Theorique des Liquides*, Gauthier-Villars et C^{ie}, Paris, 1873.
[49]Rayleigh, Lord, "On the Instability of Jets," *Proceedings of the London Mathematical Society*, Vol. 10, 1879, pp. 4–13.
[50]Worthington, A. N., *A Study of Splashes*, Longmans, Green and Co., London, 1908.
[51]Yarin, A. L., and Weiss, D. A., "Impact of Drops on Solid Surfaces: Self-Similar Capillary Waves, and Splashing as a New Type of Kinematic Discontinuity," *Journal of Fluid Mechanics*, Vol. 283, 1995, pp. 141–173.
[52]Dorman, R. G., "The Atomization of a Liquid in a Flat Spray," *British Journal of Applied Physics*, Vol. 3, 1952, pp. 189–192.
[53]Taylor, G. I., "The Dynamics of Thin Sheets of Liquid III. Disintegration of Fluid Sheets," *Collected Works of G. I. Taylor*, edited by G. K. Batchelor, 1959 (Paper 32).
[54]Zaleski, S., Li, J., Scardovelli, R., and Zanetti, G., "Direct Simulation of Multiphase Flows with Density Variations," *Proceedings of the IUTAM Conference on Variable Density Low Speed Turbulent Flows* (Marseille, France), edited by L. Fulachier and F. Anselmet, Kluwer, Dordrecht, The Netherlands, 1996.
[55]Hanson, A. R., Domich, E. G., and Adams, H. S., "Shock Tube Investigation of the Breakup of Drops by Air Blasts," *Physics of Fluids*, Vol. 6, No. 8, 1963, pp. 1070–1080.
[56]Wu, P. K., Ruff, G. A., and Faeth, G. M., "Primary Breakup in Liquid-Gas Mixing Layers," *Atomization Sprays*, Vol. 1, 1991, pp. 421–440.
[57]El-Shanawany, M. S., and Lefebvre, A. H., "Airblast Atomization: Effect of Linear Scale on Mean Drop Size," *Journal of Energy*, Vol. 4, No. 4, 1980, pp. 184–189.
[58]Rizk, N. K., and Lefebvre, A. H., "The Influence of Liquid Film Thickness on Airblast Atomization," *Transactions of the American Society of Mechanical Engineers*, Vol. 102, 1980, pp. 706–710.
[59]Kolmogorov, A. N., "On the Breakage of Drops in a Turbulent Flow," *Doklady Akademii Nauk SSR*, Vol. 66, No. 5, 1949, pp. 825–828.
[60]Keller, F., Li, J., Vallet, A., Vandrome, D., and Zaleski, S., "Direct Numerical Simulations of Interface Breakup and Atomization," *Proceedings of the ICLASS 94 Conference* (Rouen, France) 1994, pp. 56–61 (Paper I-8).
[61]Taylor, G. I., "The Shape and Acceleration of a Drop in a High-Speed Air Stream," *Collected Works of G. I. Taylor*, edited by G. K. Batchelor, 1959 (Paper 50).
[62]Gicquel, P., Brisson, E., and Vingert, L., "Experimental Investigation of a LOX Spray Under Hot Fire Conditions," *Proceedings of the ICLASS 97 Conference* (Seoul, Republic of Korea), Begell House, New York, 1997, pp. 521–526.
[63]Dahm, W. J. A., and Dimotakis, P. E., "Measurements of Entrainment and Mixing in Turbulent Jets," *AIAA Journal*, Vol. 25, No. 9, 1987, pp. 1216–1223.